Journal of Magnetic Resonance 193 (2008) 49–53

Contents lists available at ScienceDirect

Journal of Magnetic Resonance

journal homepage: www.elsevier.com/locate/jmr

# Secondary signals in two-frequency nuclear quadrupole resonance on $^{14}N$ nuclei with $I = 1$

G.V. Mozzhukhin [a,c], B.Z. Rameev [b,c,*], N. Doğan [c], B. Aktaş [c]

[a] Immanuel Kant State University of Russia, 236016 Kaliningrad, Russian Federation
[b] Kazan Physical-Technical Institute, 420029 Kazan, Russian Federation
[c] Department of Physics, Gebze Institute of Technology, Istanbul Str. 101, P.B. 141, 41400 Gebze-Kocaeli, Turkey

ARTICLE INFO

*Article history:*
Received 12 December 2007
Revised 5 April 2008
Available online 11 April 2008

*Keywords:*
Nuclear quadrupole resonance
Multifrequency methods
Spin–echo
Explosive detection

ABSTRACT

Our experimental and theoretical studies show that using two-frequency excitation of $^{14}N$ nuclei it is possible to observe secondary NQR signals at one of the three possible transitions due to irradiation of another adjacent transition. As a result of the pulse sequence applied to the adjacent transition the spin–echo signals on the detected transition are observed after essential time interval from the initial single pulse on this frequency. Experiments have been performed on the $^{14}N$ nuclei in the sodium nitrite ($NaNO_2$) and the military explosive hexahydro-1,3,5-trinitro-s-triazine $C_3H_6N_6O_6$ (RDX).



## 1. Introduction

Nuclear quadrupole resonance (NQR) of $^{14}N$ nuclei has an essential potential in the detection of explosives, narcotic materials and illegal drugs [1,2]. NQR frequencies of a resonating nucleus depend on the crystal electrical field gradient (EFG) produced by neighboring charges of a crystal host. Since the EFG is the unique parameter of a specific crystalline material, it is possible to identify various chemical compounds by their NQR spectra. However, a practical application of NQR for the detection is still a very challenging task mainly due to a very low signal to noise ratio (SNR) achieved to date. This stimulates an interest to the further researches in NQR methods including various modifications of excitation techniques. For the EFG characterized by non-zero asymmetry parameter ($\eta \neq 0$) the nuclear spin $I = 1$ of the $^{14}N$ nucleus has three energies levels and, as a result, there are three NQR transition frequencies: $\nu_1$, $\nu_2$, $\nu_3$. Thus it is possible to apply two/three-frequency NQR methods, that is to excite two or even three NQR transitions simultaneously. An advantage of two/three-frequency excitation from the practical point of view is mainly related to possible gain in the reliability of the material detection by NQR as well as in the better SNR of low-frequency NQR spectra [3,4]. Moreover, there are some prospects of the multifrequency NQR methods to realize in practice the quantum computations [5].

An application of two-frequency pulse irradiation to the adjacent NQR transitions results in the NQR signals, which are different from a conventional single-frequency NQR. It is convenient to refer to these signals by the term of "secondary echo" which has been introduced in Ref. [6]. However, one has to take into account the signals of free induction decay arising due to multifrequency excitation as well [7]. Thus we also use in this work the more common term of secondary NQR signals to consider all signals that may appear as result of the multifrequency excitation.

An experimental observation of the secondary NQR signals of $^{14}N$ in $NaNO_2$ has been performed previously mainly to demonstrate an opportunity of unambiguous assigning the adjacent NQR transitions [7,8]. Later an interest of researchers concentrated on observation of the secondary echo on the third NQR frequency under the two-frequency irradiation [4,6], as well as on possibility to use two-frequency multipulse sequences [9,10]. In this respect it is worth to note that there is a number of the publications including NQR on $^{14}N$ nuclei, where the secondary echoes [3,7,9–12] have been predicted. However, in many cases these signals have not observed experimentally due to some reasons. One of these reasons is the difference in the relaxation parameters of real substances and those used in the model calculations. Furthermore, usually such calculations are performed without taking into account relaxation processes of the system and based on the density matrix formalism in one particle approach [3,4,6–8,11,12]. It is accepted that the relaxation times are essentially longer that the time of experiment. However, it is not fulfilled, e.g. in the case of hexahydro-1,3,5-trinitro-s-triazine $C_3H_6N_6O_6$ (RDX). It has been shown that for this substance the results of the model calculations cannot be applied

* Corresponding author. Address: Department of Physics, Gebze Institute of Technology, Istanbul Str. 101, P.B. 141, 41400 Gebze-Kocaeli, Turkey. Fax: +90 262 6538490.
*E-mail address:* rameev@gyte.edu.tr (B.Z. Rameev).

1090-7807/$ - see front matter © 2008 Elsevier Inc. All rights reserved.
doi:10.1016/j.jmr.2008.04.015

even in the simplest case of secondary signals related with the coherence transfer between adjacent transitions [13]. Another reason is the experimental complications that appear in multifrequency NQR experiments. The detector construction has to include two or three resonance circuits with the operation frequencies between 0.4 and 6 MHz. Besides, the crosstalk between these circuits should be negligible, that is especially important at the frequencies below 1 MHz.

An interest to the two/three-frequency NQR was initially motivated by intention to exclude an influence of transient processes in the detection devices by registration of the signal on the third non-irradiated transition, while the other two transitions are under the radiofrequency excitation [3,4]. For that the complicated system of three mutually orthogonal coils, two-channel transmitter with excitation frequencies $\nu_1$ and $\nu_2$, and the receiver operating on the third-frequency frequency $\nu_3$ have been used [4]. However it is very challenging task to apply such technique for the distant detection of explosives especially due to problems in the detector design. For the practical application one has also to take into account the significant drift of NQR frequency with sample temperature. Thus, it is quite complicated task to control the system having three degree of freedom; therefore it is highly desirable to simplify such system as much as possible but saving its potential advantages.

In this work, we concentrate on the two-frequency NQR technique with registration of the secondary NQR signal at one of the irradiated transitions. We have observed the secondary signal appearing after excitation of the transition ($\nu_-$), detected however not directly, but after essential time interval during which the adjacent transition ($\nu_+$) is excited. It has been shown that the obtained results are similar to the three-frequency NQR on $^{14}$N [4]. We have tested this sequence on the different compounds: the sodium nitrite ($NaNO_2$) and the explosive compound hexahydro-1,3,5-trinitro-s-triazine $C_3H_6N_6O_6$ (RDX). It has been demonstrated that application of the sequences similar to the applied in our work may be prospective to use in NQR detection of various nitrogen compounds, such as explosives, narcotics and illegal substances.

## 2. Experimental procedures

NQR experiments have been performed on two-frequency pulse mode spectrometer with operating frequency range of 0.5–18 MHz. The spectrometer consists of: (1) *Apollo Tecmag* NQR/NMR console (0.1–100 MHz) with two-channel transmitter and one-channel receiver modules; (2) two *Tomco BT-00500-Beta* power amplifiers with the output power up to 500 W and the frequency range of 0.5–18 MHz; and (3) two-frequency detector unit. The detector unit includes a home-made low noise single channel preamplifier and the system of two orthogonal saddle coils *x* and *y*, each of them is connected in the serial resonance circuit tuned for the resonance frequencies $\nu_+$ and $\nu_-$, respectively. The loaded *Q*-factors of the resonance circuits of the detector unit used in the NQR measurements of $NaNO_2$ are 74 for the frequency $\nu_-$ and 60 for $\nu_+$, while the *Q*-factor of the detector used for RDX is about 100.

The sample of RDX (hexahydro-1,3,5-trinitro-s-triazine) $C_3H_6N_6O_6$ has been the powder with weight about 400 g, placed inside a cubic container with the edge size of 100 mm. The room temperature NQR parameters of RDX sample as follows. The asymmetry parameter $\eta = 60.24\%$, and the resonance frequencies are $\nu_+ = 5048$ kHz (i.e. transition between the NQR energy states $0 \rightarrow +1$) and $\nu_- = 3359$ kHz ($0 \rightarrow -1$). The relaxation parameters on the frequency $\nu_+$: the longitudinal relaxation time is $T_1 = 10$ ms, transverse time is $T_2 = 8$ ms, and $T_2^* = 0.5$ ms ($T_2^*$ is the relaxation time related to the linewidth [2]; $T_2^* = 1/\pi\Delta\nu_{1/2}$; $\Delta\nu_{1/2}$ is the full width at half height). The relaxation parameters on the frequency $\nu_-$: the longitudinal relaxation time is $T_1 = 10$ ms, transverse time is $T_2 = 4$ ms, and $T_2^* = 0.4$ ms.

The sample of sodium nitrite ($NaNO_2$) is the powder with weight of 20 g placed inside the teflon ampoule. The room temperature NQR parameters of this substance (see, e.g. [14]) as follows. For the resonance frequency $\nu_+ = 4640$ kHz the longitudinal relaxation time is $T_1 = 90$ ms, the transverse time is $T_2 = 5.3$ ms, and $T_2^* = 2.0$ ms. For the resonance frequency $\nu_- = 3601$ kHz the longitudinal relaxation time is $T_1 = 280$ ms, the transverse time is $T_2 = 3.3$ ms, and $T_2^* = 2.6$ ms.

## 3. Theoretical model

Hamiltonian for NQR energy levels of nuclear spin $I = 1$ is written as follows [15]:

$$H_Q = \frac{e^2Qq}{4}\left[3I_z^2 - I^2 + \frac{\eta}{2}\left(I_+^2 + I_-^2\right)\right], \tag{1}$$

where $I_\pm = I_x \pm iI_y$, and $I_x$, $I_y$, $I_z$ are the components of nuclear spin operator in the principal axes system of the EFG tensor, $\eta$ is the asymmetry parameter of the EFG, $eq$ is the field gradient, and $Q$ is the quadrupole moment of the $^{14}$N nucleus. Transition frequencies determined by the Hamiltonian are

$$\omega_0 = \frac{e^2Qq\eta}{2\hbar}; \quad \omega_+ = \frac{e^2Qq}{4\hbar}(3+\eta); \quad \omega_- = \frac{e^2Qq}{4\hbar}(3-\eta), \tag{2}$$

where $\omega_+ = 2\pi\nu_+$ corresponds to the transition between the levels labeled as + and 0 ($+ \leftrightarrow 0$), $\omega_- = 2\pi\nu_-$—to the transition ($- \leftrightarrow 0$), and $\omega_0 = 2\pi\nu_0$—to the transition ($+ \leftrightarrow -$). Fig. 1 shows the NQR energy level splittings.

In this work, we study the sequence presented in Fig. 2. The pulse duration is considered to be much shorter than the relaxation time of the quadrupole system. In this case one can use the density matrix solutions neglecting the relaxation terms. Moreover, the duration of pulses applied in the sequence is considered as negligibly small comparing with the time intervals between the pulses. The time evolution of the signals was calculated using the density matrix approach in the resonance approximation [3,12].

$$i\hbar\frac{\partial\rho}{\partial t} = [H,\rho] = H\rho - \rho H, \tag{3}$$

where $\rho$ is the density matrix, $i = \sqrt{-1}$, and $H$ is the Hamiltonian of the NQR system

$$\begin{aligned} H &= H_{1x} + H_{1y} + H_Q, \\ H_{1x} &= \gamma\hbar\bar{I}_{1x}\overline{H}_x\cos\omega_+ t, \\ H_{1y} &= \gamma\hbar\bar{I}_{1y}\overline{H}_y\cos\omega_- t \end{aligned} \tag{4}$$

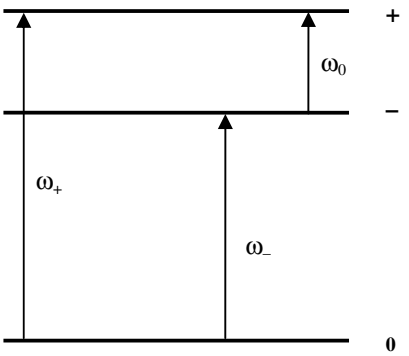


**Fig. 1.** The $^{14}$N NQR energy levels.

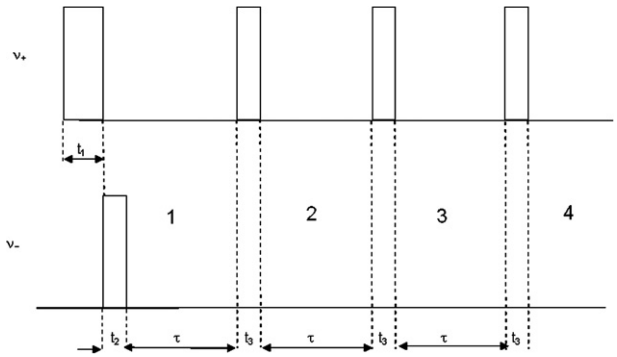


**Fig. 2.** Two-frequency sequence with the secondary NQR signals detected on the transition $\nu_-$: the sequence consists of the first two-frequency pulses on $\nu_+$ and $\nu_-$ followed by the pulses on $\nu_+$. The zero-time corresponds to the beginning of the first pulse.

where $\gamma$ is the giromagnetic ratio; $H_x$ and $H_y$ are the orthogonal components of the radiofrequency magnetic field created by two-frequency coils $x$ and $y$. We take into account the random orientation of the powder particles by the following operators $I_{1x}$ and $I_{1y}$:

$$\bar{I}_{1x} = \bar{I}_x \cos\alpha_x + \bar{I}_y \cos\beta_x + \bar{I}_z \cos\delta_x,$$
$$\bar{I}_{1y} = \bar{I}_x \cos\alpha_y + \bar{I}_y \cos\beta_y + \bar{I}_z \cos\delta_y,$$

where $\alpha_x$, $\beta_x$, $\delta_x$ and $\alpha_y$, $\beta_y$, $\delta_y$ are the angles of EFG of individual particle with respect to the axis of $x$ and $y$ coils, respectively.

As was mentioned in Section 2, one of the two mutually orthogonal coils is effective on the frequency $\nu_+$ ($I_x$ spin operator), while another one operates on the frequency $\nu_-$ ($I_y$ spin operator).

The solutions for the secondary signals on $\nu_-$ for the consecutive observation windows (see Fig. 2) are the following:

1. In the first observation window after irradiation by a pulse with the frequency $\nu_+$ (pulse duration is $t_1$) and a pulse with the frequency $\nu_-$ (pulse duration is $t_2$), the nuclear magnetization detected on the frequency $\nu_-$ is

$$\langle I_y\rangle_1 \propto \frac{\hbar\omega_-}{kT}\sin(2\gamma H_y t_2\cos\beta_y) \times\left[1-\frac{\omega_+}{\omega_-}\sin^2(\gamma H_x t_1\cos\alpha_x)\right]\sin\omega_-(t-t_1-t_2), \quad (5)$$

where $k$ is the Boltzmann constant, $T$ is the temperature. One could compare Eq. (5) with the solution for the free induction decay signal (i.e. after a single pulse on the frequency $\nu_-$) to see an appearance of additional factor that decreases the signal magnitude in the first window

$$\langle I_y\rangle \propto \left[1-m\cdot\sin^2(\gamma H_x t_1\cos\alpha_x)\right]\langle I_{y0}\rangle, \quad (6)$$

where $m=\frac{\omega_+}{\omega_-}$.

2. In the second observation window after irradiation by a pulse with the frequency $\nu_+$ and duration $t_3$, the nuclear magnetization detected on the frequency $\nu_-$ is

$$\langle I_y\rangle_2 \propto -\frac{\hbar\omega_+}{kT}\sin(2\gamma H_x t_1\cos\alpha_x)\sin(\gamma H_y t_2\cdot\cos\beta_y)\sin(\gamma H_x t_3\cdot\cos\alpha_x) \times\sin\omega_-(t-m\tau-t_1-t_2-t_3). \quad (7)$$

3. In the third observation window, after the pulse repetition with the same parameters ($\nu_+$ and $t_3$) the nuclear magnetization detected on the frequency $\nu_-$ is

$$\langle I_y\rangle_3 \propto -\frac{1}{2}\cdot\frac{\hbar\omega_+}{kT}\sin(2\gamma H_x t_1\cos\alpha_x)\sin(\gamma H_y t_2\cdot\cos\beta_y) \times\sin(2\gamma H_x t_3\cos\alpha_x)\cdot\sin\omega_-(t-2m\tau-t_1-t_2-2t_3). \quad (8)$$

4. In the fourth observation window, the nuclear magnetization is given as follows:

$$\langle I_y\rangle_4 \propto -\frac{1}{2}\cdot\frac{\hbar\omega_+}{kT}\sin(2\gamma H_x t_1\cos\alpha_x)\cdot\sin(\gamma H_y t_2\cos\beta_y) \times\sin(2\gamma H_x t_3\cos\alpha_x)\cdot\cos(\gamma H_x t_3\cos\alpha_x) \times\sin\omega_-(t-3m\tau-t_1-t_2-3t_3). \quad (9)$$

5. In the fifth observation window, after the pulse repetition with the same parameters ($\nu_+$ and $t_3$) the nuclear magnetization detected on the frequency $\nu_-$ is

$$\langle I_y\rangle_5 \propto -\frac{1}{2}\cdot\frac{\hbar\omega_+}{kT}\sin(2\gamma H_x t_1\cos\alpha_x)\sin(\gamma H_y t_2\cos\beta_y) \cdot\sin(2\gamma H_x t_3\cos\alpha_x)\cdot\cos^2(\gamma H_x t_3\cos\alpha_x) \times\sin\omega_-(t-4m\tau-t_1-t_2-4t_3). \quad (10)$$

Thus the pulse sequence applied on the frequency $\nu_+$ with the time $\tau$ between the pulses result in appearance of the secondary echo signals after each excitation pulse in the time instants $n\cdot(\omega_+/\omega_-)\tau$, where the pulse number $n$ starts to count only after the action of the first two-frequency couple of pulses. We have to note that the effect of the transverse relaxation will decrease amplitude of signals as a function of $n$. This effect starts to be important only for higher $n$ values and it has not been taken into account in our calculations.

It should be noted the signals induced due to the nuclear magnetization precession are given by

$$S_y \propto \cos\beta_y\frac{\mathrm{d}\langle I_y\rangle_n}{\mathrm{d}t}. \quad (11)$$

Eq. (11) shows that the magnitude of the secondary signals will be proportional to $\nu_+\nu_-$, where $\nu_-$ will appear due to the fact that the current in the coil is the derivative of magnetic flux created by the NQR signal magnetization.

One could obtain using the NQR frequencies that for RDX $m\approx 1.5$, while for $NaNO_2$ $m\approx 1.29$. From Eqs. (7)–(10) it follows that for higher $n$ values the secondary echo signals appear not in the window just after to the applied pulse but observed in the next windows. For instance, Eq. (7) for RDX shows that the maximal signal has to be in the center of the second observation window, while Eq. (8) results in maximum of NQR signal for the third observation window just before the next transmission pulse. In the fourth window the tail of the signal appeared in the previous window may be still observable, while the echo due to the last excitation evolves only in the next, firth window. It is remarkable that after the second exciting pulse the signal magnitudes (Eqs. (7)–(10)) became proportional to the frequency of the highest frequency $\omega_+$, but not to $\omega_-$ as in the usual single-frequency sequence.

For RDX the experimental results are presented in Fig. 3. It is clear in Fig. 3a that the FID signal appeared in the first observation window is not observed in the next windows. However for the case of the two-frequency excitation, the secondary NQR signals appear in the next observation windows. The characteristic time of their damping is very close to the time of transverse relaxation $T_2$. After firth pulse no NQR signal is observed in the window. The signal observed has the form of FID that is not expected from our calculations. We think that for RDX the relaxation parameter $T_1$ as well as the $m$ value is so, that the results of our calculations (Eqs. (7)–(10)) have to be modified further in order to be comparable with experimental results. Because in the case of RDX the ratio of the observation time to the relaxation time $T_1$ is about 30–40%, which is not enough to neglect the influence of $T_1$ in this particular case. Besides one can note that in RDX a value of $T_2$ is very close to $T_1$, that makes another complication to create the echo signal in RDX.

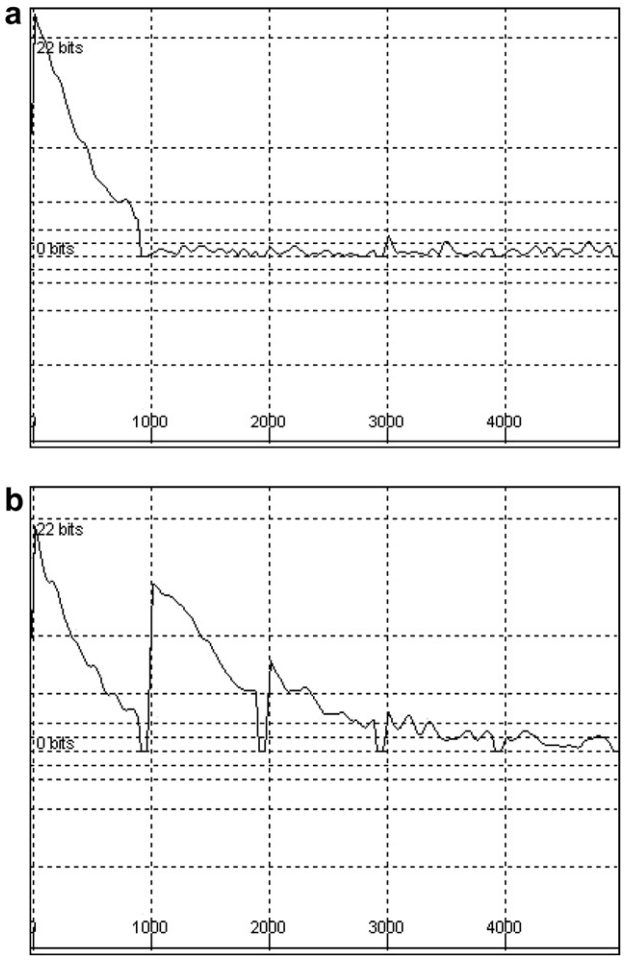


**Fig. 3.** NQR signals registered for RDX on the transition $\nu_{-} = 3359$ kHz. The first pulse duration is $t_1 = 300$ μs, the length of all other pulses is $t_2 = t_3 = 250$ μs, time interval between the pulses is 1100 μs, the observation window time is 1000 μs. There are five observation windows; number of scan repetitions is 1000. (a) The single-frequency FID signal on $\nu_{-} = 3359$ kHz (the magnitude of the signal); (b) the secondary echo signals (the signal magnitude). The tick labels on the time scales of the figures are in μs.

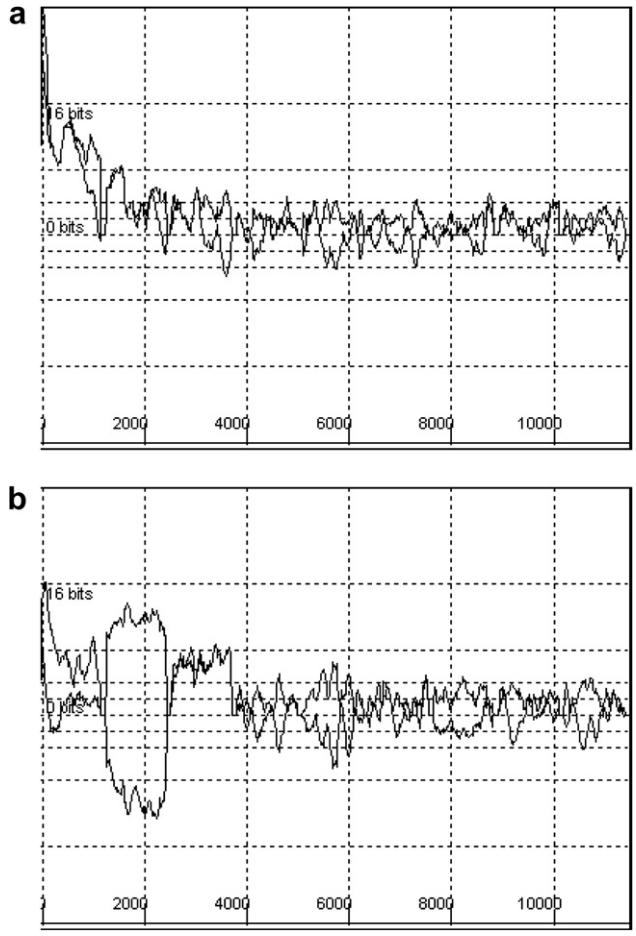


**Fig. 4.** NQR signals registered for $NaNO_2$ on the transition $\nu_{-} = 3600$ kHz. The pulse duration of all pulses is $t_2 = t_3 = 200$ μs, time interval between the pulses is 1680 μs, the observation window time is 1280 μs. There are nine *observation windows*; number of scan repetitions is 1000. (a) The single-frequency FID signal on $\nu_{-} = 3600$ kHz (the magnitude of the signal); (b) the secondary echo signals (the signal magnitude). The tick labels on the time scales of the figures are in μs.

It is interesting to compare these results with NQR measurements of $NaNO_2$ (Fig. 4). As was mentioned above this sample has the ratio $m = 1.29$. As seen from Eq. (9) the secondary signal after the action of the fourth pulse on the frequency $\nu_{+}$ appears at the moment $t \approx 3.9\tau + t_1 + t_2 + 3t_3$. However this moment coincides with the time of the application of the next fifth pulse ($t \approx 4\tau + t_1 + t_2 + 3t_3$). This well corresponds to the experimental observations in Fig. 4b, where almost zero signal observed in the fourth observation window.

We suppose that for the appropriated description of the behavior observed in the next windows one should take into account the relaxation effects, neglected in our model. As was mentioned above the Eqs. (5)–(10) were obtained in the approximation of the long relaxation times which are larger comparing the observation time. However $T_2 = 5.3$ and 3.3 ms for the frequencies $\nu_{+}$ and $\nu_{-}$, respectively, so relaxation effects became important for the higher observation windows and it should be a subject of further studies. For instance we see some week signal in the *fifth* window, while the secondary signal after the action of the fifth pulse on the frequency $\nu_{+}$ should appear at the moment $t \approx 5.2\tau + t_1 + t_2 + 4t_3$ (Eq. (10)), that is in the *sixth* window. Therefore, we believe that our theoretical calculations match enough well to the experimental results on $NaNO_2$ only up to the fourth observation window inclusively.

Thus, the shape of the secondary signals for $NaNO_2$ and RDX reveals an essential effect of the relaxation parameters. The secondary signals in RDX shows the FID character which is worth to be a subject of separate study. However, in the case of RDX we observe that an application of the pulse with frequency $\nu_{-}$ in the studied sequence results in abrupt decrease in the magnitude of the signals on $\nu_{+}$ comparing with the single-frequency sequence on the same transitions, that reflects the polarization transfer to the adjacent transition with frequency $\nu_{-}$.

## 4. Conclusion

Our experimental and theoretical studies show that using the two-frequency excitation of energy levels of $^{14}N$ quadrupolar nuclei ($I = 1$) it is possible to observe the NQR signals on the one of the excited NQR transitions, which are similar to the secondary signals on the third non-irradiated transition (see [4,6]). That is possible to excite such two-frequency steady-state in the system, which is locked by a continuous pulse series applied to one of the adjacent transitions and detected on another transition due to the secondary signals. In fact we observe a set of the echo signals as result of a "single" pulse on the observed transition. Theoretical calculations allow us to explain the observed features of the secondary signals in $NaNO_2$. It is remarkable that the signal magnitude is affected

by polarization transfer from the transition with higher frequency. Owing to pulse series applied to the adjacent transition it was possible to observe the secondary echo signals for the time interval of about the transverse relaxation time, $T_2$, after the pulse excitation applied on the detected frequency. Thus, our studies reveal that the sequences similar to the used in our work may be prospective to use in the NQR detection of various nitrogen compounds, such as explosives, narcotics and illegal substances.

## Acknowledgments

Authors acknowledge the support under NATO CLG (No. 982346) and NATO SfP (No. 982836) programs. This work was also supported by the grant No. 106T321 of TÜBİTAK (The Scientific and Technological Research Council of Turkey) and in part by the grant No. 00062.STZ.2007-1 of Ministry of Industry and Trade of Turkey.

## References

[1] J.B. Miller, G.A. Barrall, Explosives detection with nuclear quadrupole resonance, Am. Sci. 93 (2005) 50–57.
[2] A.N. Garroway, M.L. Buess, J.B. Miller, B.H. Suits, A.D. Hibbs, G.A. Barrall, R. Matthews, L.J. Burnett, Remote sensing by nuclear quadrupole resonance, IEEE Trans. Geosci. Remote Sensing 39 (6) (2001) 1108–1118.
[3] G.V. Mozjoukhine(Mozzhukhin), The two-frequency nuclear quadrupole resonance for explosives detection, Appl. Magn. Reson. 18 (4) (2000) 527–535.
[4] K.L. Sauer, B.H. Suits, A.N. Garroway, J.B. Miller, Three frequency nuclear quadrupole resonance of spin-1 nuclei, Chem. Phys. Lett. 342 (3–4) (2001) 362–368.
[5] A.R. Kessel, V.L. Ermakov, Virtual qubits—many levels instead of many particles, JETP 117 (3) (2000) 517–525.
[6] K.L. Sauer, B.H. Suits, A.N. Garroway, J.B. Miller, Secondary echoes in three-frequency nuclear quadrupole resonance of spin-1 nuclei, J. Chem. Phys. 118 (11) (2003) 5071–5081.
[7] G.V. Mozjoukhine (Mozzhukhin), Application of the spherical tensor method for two frequency pure NQR of spin $I = 1$ nuclei, Appl. Magn. Reson. 22 (2002) 31–46.
[8] V.S. Grechishkin, G.V. Mozzhukhin, N.Y. Sinyavskii, E.V. Yurepina, Two-frequency saturation in pulsed NQR of $^{14}$N, Russ. Phys. J. 31 (8) (1988) 647–649 (Transl. from Izvestiya Vysshikh Uchebnykh Zavedenii, Fizika, No. 8, pp. 48–51, August 1988).
[9] D.Y. Osokin, R.R. Khusnutdinov, V.A. Shagalov, Two-frequency multiple-pulse sequences in nitrogen-14 NQR, Appl. Magn. Reson. 25 (3–4) (2004) 513–521.
[10] D.Y. Osokin, R.R. Khusnutdinov, Theory of two-frequency excitation in $^{14}$N NQR, Appl. Magn. Reson. 24 (2) (2003) 145–156.
[11] V.S. Grechishkin, N.Y. Sinyavskiĭ, Remote nuclear quadrupole resonance in solids, Phys. Usp. 36 (10) (1993) 980–1003.
[12] V.S. Grechishkin, V.P. Anferov, N.J. Sinjavsky, Adiabatic demagnetization and two-frequency methods in $^{14}$N NQR spectroscopy, in: J.A.S. Smith (Ed.), Advances in Nuclear Quadrupole Resonance, vol. 5, Wiley, London, 1983, pp. 1–51.
[13] G.V. Mozzhukhin, A.V. Bodhya, V.V. Fedotov, Effect of $^{14}$N nucleus capture in nuclear quadrupole resonance at small relaxation parameters, Russ. Phys. J. 48 (4) (2005) 383–386.
[14] A.N. Garroway, M.L. Buess, J.P. Yesinowski, J.B. Miller, Narcotics and explosives detection by $^{14}$N pure NQR, SPIE Proc. Ser. 2092 (1993) 318–327.
[15] C.P. Slichter, Principle of Magnetic Resonance, Springer, New York, 1996.